H-mode threshold and dynamics in the National Spherical Torus Experiment[a]

C. E. Bush,[1,b] M. G. Bell,[2] R. E. Bell,[2] J. Boedo,[3] E. D. Fredrickson,[2] S. M. Kaye,[2]
S. Kubota,[4] B. P. LeBlanc,[2] R. Maingi,[1] R. J. Maqueda,[5] S. A. Sabbagh,[6]
V. A. Soukhanovskii,[2] D. Stutman,[7] D. W. Swain,[1] J. B. Wilgen,[1] S. J. Zweben,[2]
W. M. Davis,[2] D. A. Gates,[2] D. W. Johnson,[2] R. Kaita,[2] H. W. Kugel,[2] K. C. Lee,[8]
D. Mastrovito,[2] S. Medley,[2] J. E. Menard,[2] D. Mueller,[2] M. Ono,[2] F. Paoletti,[6] H. Park,[2]
S. J. Paul,[2] Y-K. M. Peng,[1] R. Raman,[9] P. G. Roney,[2] A. L. Roquemore,[2]
C. H. Skinner,[2] E. J. Synakowski,[2] G. Taylor,[2] and the NSTX Team
[1]Oak Ridge National Laboratory, Oak Ridge, Tennessee 37831
[2]Princeton Plasma Physics Laboratory, P.O. Box 451, Princeton, New Jersey 08543
[3]University of California, San Diego, San Diego, California
[4]University of California at Los Angeles, Los Angeles, California
[5]Los Alamos National Laboratory, Los Alamos, New Mexico 87545
[6]Columbia University, New York, New York 10027
[7]Johns Hopkins University, Baltimore, Maryland
[8]University of California Davis, Davis, California
[9]University of Washington, Seattle, Washington 98195

Edge parameters play a critical role in high confinement mode (H-mode) access, which is a key component of discharge optimization in present day toroidal confinement experiments and the design of next generation devices. Because the edge magnetic topology of a spherical torus (ST) differs from a conventional aspect ratio tokamak, H-modes in STs exhibit important differences compared with tokamaks. The dependence of the National Spherical Torus Experiment (NSTX) [C. Neumeyer *et al.*, Fusion Eng. Des. **54**, 275 (2001)] edge plasma on heating power, including the low confinement mode (L-mode) to H-mode (L-H) transition requirements and the occurrence of edge-localized modes (ELMs), and on divertor configuration is quantified. Comparisons between good L-modes and H-modes show greater differences in the ion channel than the electron channel. The threshold power for the H-mode transition in NSTX is generally above the predictions of a recent International Tokamak Experimental Reactor (ITER) [ITER Physics Basis Editors, Nucl. Fusion **39**, 2175 (1999)] scaling. Correlations of transition and ELM phenomena with turbulent fluctuations revealed by gas puff imaging and reflectometry are observed. In both single-null and double-null divertor discharges, the density peaks off-axis, sometimes developing prominent "ears" which can be sustained for many energy confinement times, τ_E, in the absence of ELMs. A wide variety of ELM behavior is observed, and ELM characteristics depend on configuration and fueling. © *2003 American Institute of Physics.* [DOI: 10.1063/1.1567288]

I. INTRODUCTION

A main goal of the National Spherical Torus Experiment (NSTX)[1] is to assess the attractiveness of the spherical torus (ST) for pulse lengths longer than current diffusion times. This is important since one possible advantage of operation at low aspect ratio, $A \equiv R/a$, would be a smaller size, and in turn, a lower cost reactor concept. High confinement mode (H-mode) studies are important to this goal since H-mode profiles provide the stability needed for high β long pulse operation.

Recent operation of NSTX has resulted in rapid progress in increasing performance.[2–4] This was accomplished through reduction of intrinsic magnetic field errors, improvements in machine conditioning techniques, and development of operational scenarios with gas puffing from the center stack. As a result, H-mode access and reproducibility were improved substantially.

The main advantages of the H-mode are broad density, temperature, and pressure profiles. Use of the H-mode has allowed rapid progress in increasing the toroidal beta (β_T) up to 35%,[5] where $\beta_T = \langle p \rangle / (B_{T0}^2 / 2\mu_0)$ and B_{T0} is the vacuum toroidal field at the geometric radius, due to the reduced pressure peaking factor and improved energy confinement. H-modes have also helped in sustaining high β_T ~21% for 500 ms, as a result of reduced volt-second consumption because of high bootstrap fraction.

In order to utilize H-modes to achieve the goals of NSTX, experiments were conducted to determine the parametric and configurational dependencies of the L-H power threshold and occurrence of edge-localized-modes (ELMs). This paper describes the H-mode operating window, power threshold studies, fluctuation studies, and ELM experiments.
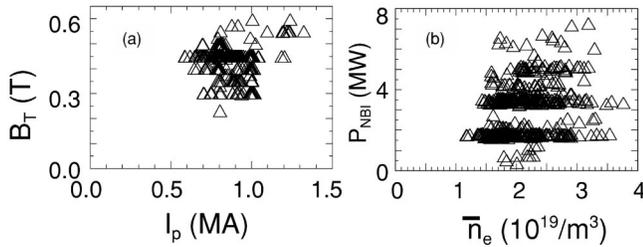
FIG. 1. The parameter ranges for the NSTX H-mode access space. (a) B_T vs I_p and (b) P_{NBI} vs n_e at the time of the L–H transition time.

FIG. 3. Time evolution of n_e and T_e profiles for the long pulse plasma of Fig. 2.

II. DESCRIPTION OF EXPERIMENT AND H-MODE PARAMETER RANGE

The H-mode results reported here were all for plasmas for which only neutral beam injection, NBI, auxiliary heating was used. H-mode results utilizing radio frequency (RF) heating were reported elsewhere.[6] H-modes were obtained in both lower single null divertor (LSN) and double null divertor (DN) configurations. The majority of shots were LSN but the DN configuration is finding increasing usage because of access to higher I/aB, and thus higher absolute β_T. However, it was observed that ~2 times higher heating power was required to access DN H-modes. During the most recent experimental campaign, no effort was made to obtain H-modes using the upper single null configuration. Also, a dedicated effort has not been made to obtain ohmically heated (OH) or center-stack limited H-modes. No H-modes were obtained in any of these three cases.

β limit studies were done mainly in the double-null divertor configuration, and pulse length extension studies in the lower single null configuration. Heating power included up to 7 MW of neutral beam injection, NBI, and 6 MW of high harmonic fast wave, HHFW, radio frequency power. The lowest aspect ratio, $A \equiv R/a$, achieved was ≥ 1.27 for $R = 0.8$ m and $a = 0.67$ m; more typically, $A \sim 1.4$–1.5 for H-mode discharges with an inner wall gap of ~10 cm. The parameter ranges for access to H modes in NSTX were wide, and this can be seen from Fig. 1, where plots of B_T vs I_p [Fig. 1(a)] and P_{NBI} vs n_e are shown. Here, n_e was the line-averaged density at the time of the L–H transition. From Fig.
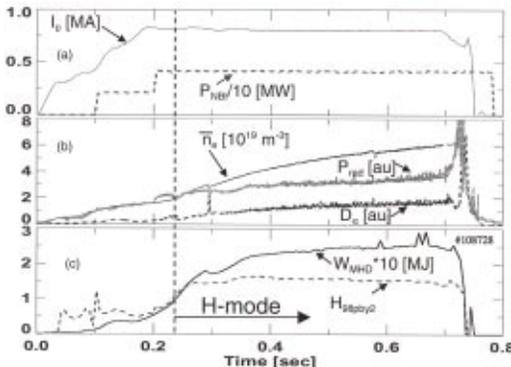
FIG. 2. Time variation of parameters for a long pulse H-mode. Including (a) machine parameters I_p and P_{NBI}, (b) plasma parameters n_e, P_{rad}, and D_α, and (c) performance parameters W_{MHD} and enhancement factor over L-mode, H_{98pby2}.
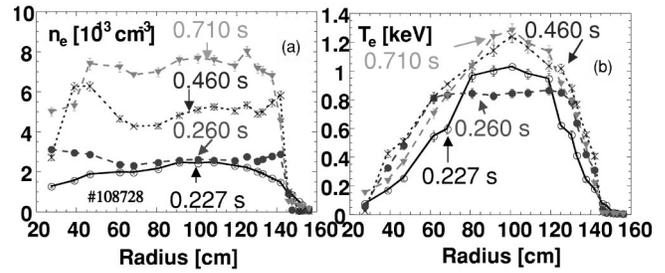
1(a) one can see the ranges for I_p and B_T; $0.6 \leq I_p \leq 1.3$ MA and $0.3 \leq B_T \leq 0.6$ T. The beam power was varied from a low of 320 kW to a high of 22 times this value, i.e., 7 MW. The range of plasma line averaged densities was $1.5 \leq n_e \leq 4.8 \times 10^{19}/m^3$ (at the L–H time). In addition $\beta_T \sim 35\%$ and $\beta_p \sim 1.4$ were obtained, and the maximum H-mode phase duration was ~500 ms (with NBI). The database plotted in Fig. 1 contains more than 500 H-mode plasmas.

The rapid progress in NSTX performance was made possible by a wall-conditioning regimen[7] consisting of a 350 °C bake-out, followed by boronization, and between shot helium glow discharge cleaning. Use of high field side (HFS) gas puff fueling served to increase ease of access to the H-mode just as was observed earlier on Mega-Ampère Spherical Tokamak (MAST).[8] The results for a high field side (HFS) vs low field side (LFS) H-mode access experiment in NSTX were recently reported.[9] It was found during HFS fueling studies that at too high a gas puff rate, H-modes did not occur, and at too low a flow rate, low density locked modes and reconnection events occurred.

A very important result for the NSTX H-mode was that not only was high performance achieved, but it could also be sustained during long duration H-modes. Figure 2 shows a long pulse (>700 ms) discharge where the L–H transition took place at 230 ms and the H-mode duration was ~500 ms. Through the duration of the H-mode, the stored energy [Fig. 2(c)] plateaued at $W_{MHD} = 250$ kJ. The energy confinement enhancement factor, H_{98pby2}, over the predictions of the ITER-98P ELMY H-mode scaling[10] remained at a steady state value of 1.5. Figure 2(b) shows that the line averaged density increased during the H-mode reaching a value of $6 \times 10^{19}/m^3$. Note that the radiated power, P_{rad}, Fig. 2(b) was fairly constant during the long duration H-mode phase, indicating that there was no significant core impurity accumulation.

One benefit of the long duration H-mode was the ability to observe profile evolution. Early NSTX H-modes[11,12] were too short for such observations. For the long pulse high performance H-mode of Fig. 2 we see that the n_e and T_e profiles evolved differently. The n_e profile of Fig. 3(a) shows the usual L-mode edge at $t = 0.227$ s. At the transition the edge n_e pedestal rose rapidly, developing an off axis peak or "ears"[13] by $t = 0.260$ s. The early profiles were hollow. The n_e profile evolved with the core filling in faster than the
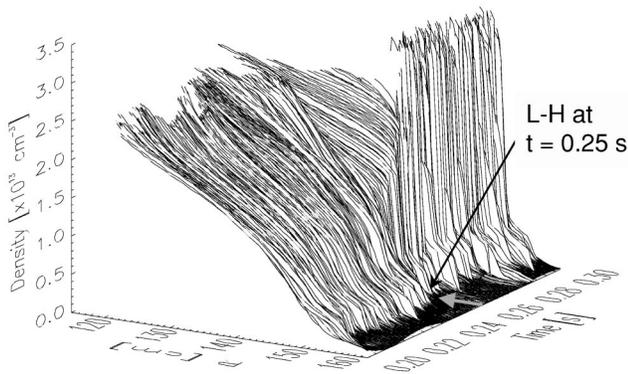
FIG. 4. Fast scanning reflectometer profile data for an NSTX shot with an L–H transition at $t = 0.25$ s. The high spatial and temporal resolutions in the edge plasma are clearly seen.

edge, and finally becoming flat with no "ear" features. In general, the n_e profile filled in within 300 to 500 ms. On the other hand, the T_e profile, Fig. 3(b), was flattened and broadened significantly ($t = 0.26$ s) just after the transition. Initially it remained broad but later became peaked. The flat n_e profile and broad T_e profile resulted in a broad pressure profile with low pressure peaking factor $F_p = p_e(0)/\langle p_e \rangle \lesssim 2$. The NSTX H-mode developed a very steep electron density gradient at the edge that evolved rapidly at the L–H transition. A fast scanning edge reflectometer was used on NSTX to follow the dynamics of the edge density with much better time resolution than available with the Thomson scattering diagnostic. However, the 20 point Thomson scattering (TS) data of Fig. 3 do provide sufficient spatial resolution for resolving the pedestal; ∼6–8 points usually define the n_e pedestal "ear" and height. At the plasma edge the TS points are ∼2.5 cm apart and are acquired at a rate of 60 Hz. Reflectometer data for a different H-mode is shown in Fig. 4, illustrating the high time (profile every 100 μs) and spatial resolution of that diagnostic. Following the L–H transition at $t = 0.25$ s, the edge profile steepens and shifts inward as the pedestal height increases. The steep density gradient during the H-mode and evident in both the TS and reflectometer data was consistent with the concept of an edge transport
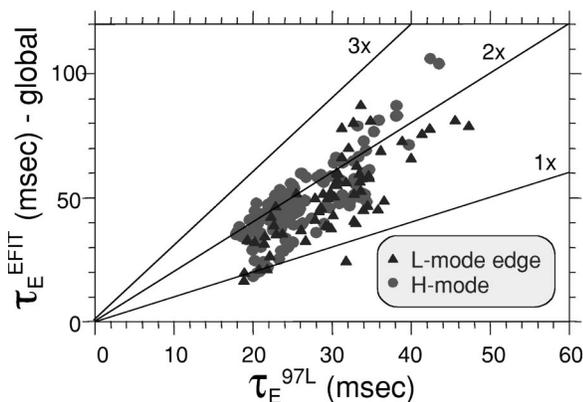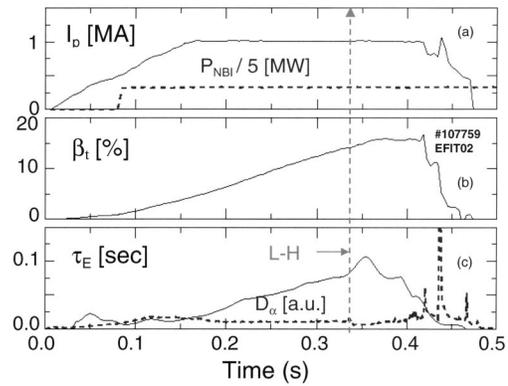
FIG. 6. Parameters for a high performance L-mode plasma in which an L–H transition occurs late in the discharge (at $t = 0.34$ s).

barrier. At the steep gradient position, the ultrasoft x-ray (USXR) array often showed accumulation of carbon. However, there often was no evidence for accumulation of impurities inside the edge barrier.

In NSTX both L-mode and H-mode plasmas achieved good confinement reproducibly. This is shown in Fig. 5, which is a plot of τ_E^{NSTX} vs τ_E^{97L} (Refs. 14 and 6) where the experimental values were taken at times when the plasma was in quasisteady state. Both L modes and H-modes occurred throughout the range of $0.75 \leqslant \tau_E^{\mathrm{NSTX}}/\tau_E^{97L} \leqslant 2.5$, with a maximum measured confinement time of 110 ms. There is significant scatter in the data as plotted in Fig. 5 indicating that τ_E^{97L} may not be a good scaling for NSTX L-mode or H-mode (as expected) data. This may indicate that transport physics in ST's are dominated by different processes than those for conventional aspect ratio tokamaks. Development of separate τ_E scalings for NSTX are in progress.

Normally in NSTX, the gain in confinement time following a transition from the usual L-mode confinement (i.e., 97 L-mode scaling) to H-mode was >50%, as in conventional aspect ratio tokamaks. In NSTX, it was of interest to capitalize on the high performance L-mode by obtaining the same percentage gain in performance from L to H. However, very often the gain in going from a high performance L-mode to H-mode was rather modest. An example of this behavior is the discharge[3] of Fig. 6, for which the time variation of I_p and P_{NBI} [Fig. 6(a)], β_T [Fig. 6(b)], and τ_E and D_α [Fig. 6(c)] are plotted. In this case, the L–H transition was late in the discharge (∼0.34 s) and the L-mode performance at the time of transition was high. At the transition there was a transient increase in τ_E which quickly rolled over; β_T increased from ∼13% before the transition to a final plateau value of ∼16% during the H-mode phase. Possible explanations for the reduced gain in performance are based on profile effects and MHD activity. Mirnov coil data showed turn on of an $n = 1$ mode, believed to be core localized, just before rollover of τ_E at $t = 0.35$ s. However, such a rollover does not always occur for similar MHD activity.

Additional insight was obtained by comparing plasma profiles before and after the L–H transition (Fig. 7). A big difference appeared to be in the ion channel, based on T_i and

FIG. 5. Comparison of confinement in NSTX to that for the ITER EPS97-L-mode scaling. The average for the NSTX H-mode is 1.5× EPS97-L-mode, and ranges from 0.75 to 2.5 times the L-mode scaling.
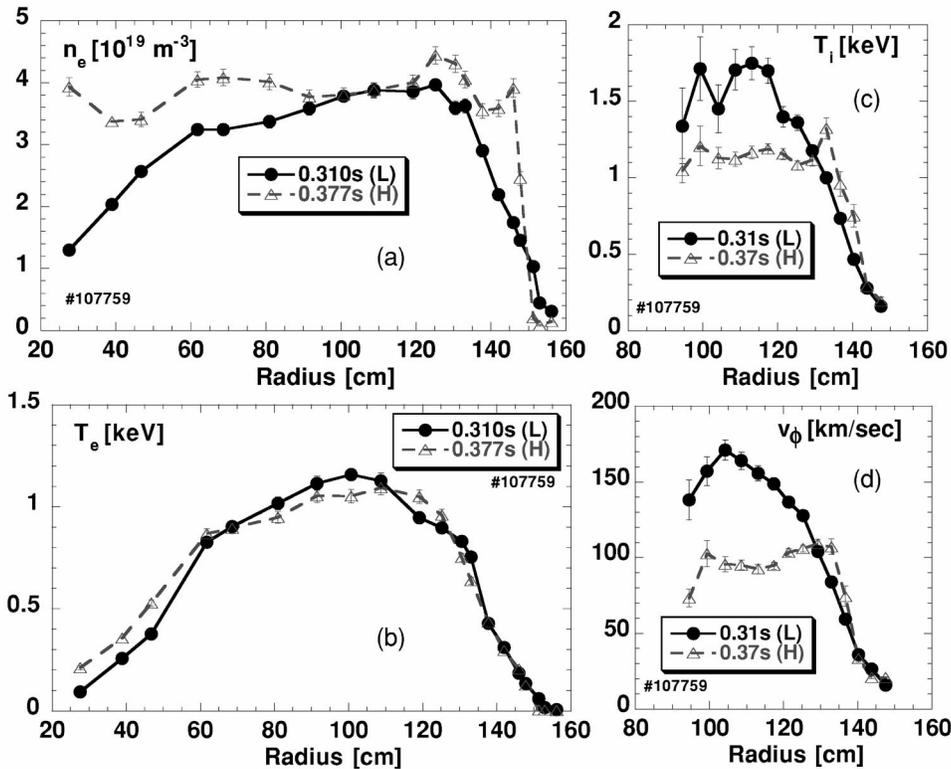
FIG. 7. Comparison of profiles for the L-mode just before the transition with the H-mode shortly after the transition. The ion channel (T_i, V_ϕ) was affected significantly.

V_ϕ profiles from the charge exchange recombination spectroscopy (CHERS) diagnostic. The profiles for the electron channel, n_e and T_e are plotted in Figs. 7(a) and 7(b). The edge density gradient ∇n_e was high and the pedestal n_e in the H-mode phase was ~4 times the L-mode edge value. The H-mode n_e profile was rather flat. There was little difference in the T_e profiles in general, though, the inner (high field side) T_e went from 100 eV in L mode to 200 eV in H mode. The H-mode T_e profile was also rather flat. On the other hand, the T_i and V_ϕ profiles [Figs. 7(c) and 7(d)] were dramatically different. The T_i profile went from peaked to flat with a much steeper edge gradient, ∇T_i, with a decrease in the core from 1.7 keV to 1.1 keV. Similarly the V_ϕ profile went from centrally peaked to flat and a central value of 170 km/s in the L-mode plasma to ~100 km/s in the H-mode phase with a steep edge gradient. Possible explanations for the resulting profiles in the H-phase include triggering of the $n=1$ MHD mode, discussed earlier, soon after (at $t = 0.35$ s) the transition that could have effectively increased the core transport. These cases were not fully understood and will require further study.

III. POWER THRESHOLD STUDIES ON NSTX

The L–H threshold power requirements for obtaining H-modes were determined for a number of parameter/configuration combinations in NSTX. This was done in a series of dedicated experiments involving scans in P_{NBI}, I_p, B_T, and n_e and in the divertor configuration. In addition, the physics of the L–H transition and the resulting characteristics of the H-mode and ELMs, were investigated as part of the power threshold experiments.

The L–H power threshold was found by reducing P_{NBI} for a given I_p, B_T, and n_e until no L–H transition occurred. The indicators for being near the threshold were very short H modes or dithers as observed in the D_α signal. Parameters for discharges of a representative threshold determination are shown in Fig. 8. In this case I_p and B_T were 0.9 MA and 0.45 T, respectively. Shown are time traces of I_p [Fig. 8(a)], P_{NBI} [Fig. 8(b)], and D_α [Fig. 8(c)]. Four discharges [indicated by 1–4 in Fig. 8(b)] of the beam power scan are presented in the figure, for three different power levels; 0.675, 1.146, and 1.636 MW. The power scan began at $P_{NBI}=1.636$ MW, using a single beam source full-on at a beam voltage of 80 kV, which was far above the threshold. The beam voltage was decreased to obtain the power levels shown in Fig. 8(b). The L–H transition, as indicated by the drop in the D_α emission, took place at essentially the same time of 0.210 ms for the three shots that showed transitions, well after the NBI turn-on time. At the lowest P_{NBI} (0.675 MW), one discharge had a short H-mode and the other no H-mode at all. This was taken to be an indication that 0.675 MW was the P_{NBI} required essentially at or very close to the threshold power. A trend evident in Fig. 8(c) is that the duration of the H-mode increased with power above the threshold, going from ~7 ms near the threshold to 50 ms at nearly twice (5/3) the threshold power and $\geq$90 ms at the highest power (2.4 times P_{NBI} at the threshold).

The example of Fig. 8 included many of the main components of the threshold determination procedure in NSTX. However, since only one beam source was required, the full means of controlling the range in power possible could not be demonstrated in Fig. 8. The extremely wide range in P_{NBI} of 320 kW to 7 MW [Fig. 1(a)] was obtained using a com-
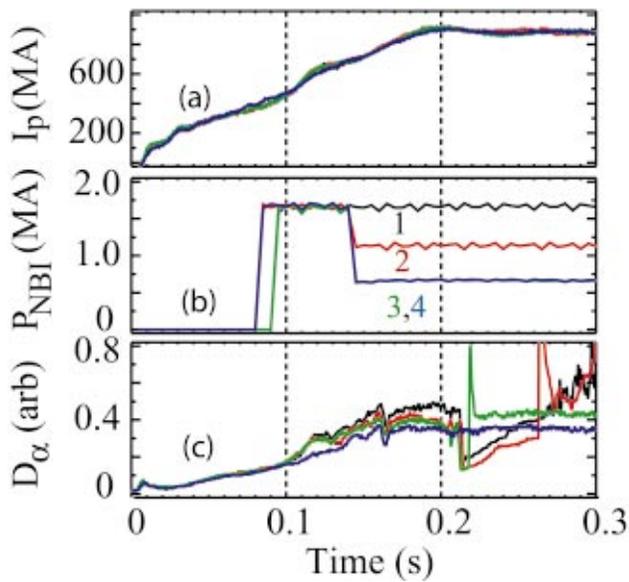
FIG. 8. (Color) Time variation of parameters for a P_{NBI} scan at I_p $=900$ kA and $B_T=0.45$ T. Note that the H-mode duration was reduced as heating power approached the L-H threshold.

FIG. 10. A clear dependence of P_{th} on plasma current is shown in this plot of $P_{LOSS}/P_{th,1}$ vs I_p. Here, $P_{LOSS} \sim 3 \times P_{th,1}$ at $I_p=0.6$ MA. The red dots are shots that had L–H transitions and the solid blue squares are L-mode shots in which H-modes were not obtained.

bination of varying the number of beam sources from 1 to 3, varying the beam voltage from ~45 kV to ~100 kV and finally by beam modulation. For the low value of 320 kW a low beam voltage of 55 kV was used and a single source was modulated using a 50% duty cycle of 10 ms beam on and 10 ms beam off. Usually as the power was increased above the

threshold, the transition time shifted forward to an earlier time, consistent with easier access to the H mode at the higher power levels.

The power threshold on NSTX has an apparent current dependence. This was seen from determinations of the threshold power (P_{th}) for L–H transitions at two different currents, 600 and 900 kA, respectively, both at a B_T $=0.45$ T and use was made of the techniques presented in Fig. 8. Results for this comparison are shown in Fig. 9, where the time variation of I_p, P_{NBI}, and D_α are given for the two cases. Modulated beam power was used to lower P_{NBI} sufficiently to obtain the result for the 600 kA case as can be seen in Fig. 9(c). The very short H-mode phases were taken as evidence that the power was close to the threshold in each case. P_{NBI} required at the threshold were 320 kW at 600 kA and 660 kW at 900 kA. The current dependence

FIG. 9. (Color) Time variation of parameters for threshold determination at two values of I_p; 600 kA and 900 kA. The short H-phase occurs near the threshold in both cases.
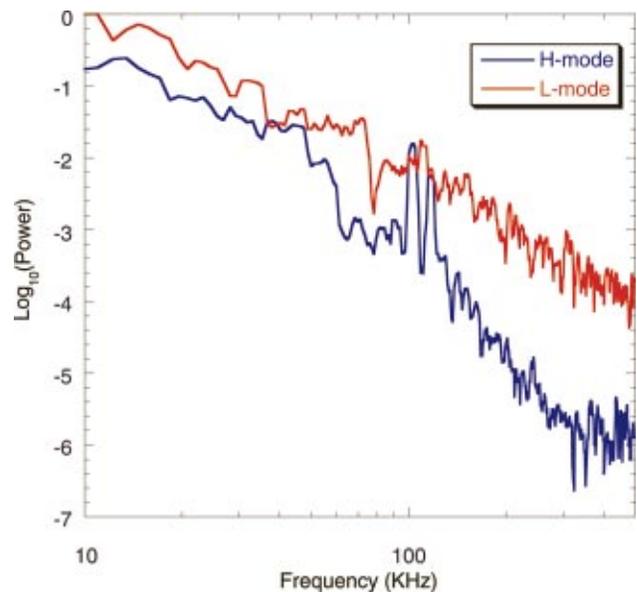
FIG. 11. (Color) Fluctuation spectra for L-mode and H-mode discharges from the broadband 6 to 26 GHz reflectometer. The amplitude of fluctuations was much lower in the H-mode than in the L-mode. A coherent mode centered at ~120 kHz was clear in the H-mode spectrum.

discussed above is not present in the scalings derived from the ITER database.

The NSTX L–H threshold powers for the discharges of Fig. 9 can be compared to values given by scalings derived from conventional aspect ratio tokamak data contained in the international L–H threshold database. The most recent scaling was given by $P_{th,1} \sim n_e^{0.61} B_T^{0.78} a^{0.89} R^{0.94}$.[15] The experimental loss power, $P_{LOSS} = P_{OH} + P_{NBI} - dW/dt - P_{FLOSS}$, (where P_{FLOSS} included the total fast ion loss power as calculated by TRANSP) was normalized to the above scaling for P_{th} and plotted versus I_p in Fig. 10 along with other L-mode and H-mode data near the threshold. In the figure, P_{LOSS} values ranged from 96 kW for $I_p = 600$ kA to 230 kW for 1 MA. As seen from Fig. 10, the threshold power levels for NSTX H modes were higher than those predicted by the scalings, even though the actual values of P_{NBI} were rather modest. The ratio at 600 kA was $P_{LOSS}/P_{th,1} \sim 2.5$, i.e., the threshold level for NSTX was 2.5 times $P_{th,1}$. At 900 kA the ratio was ~ 6.3. These results indicate the importance of including the NSTX data to determine explicit aspect ratio dependence in future threshold scalings. Adding NSTX data would be in the spirit of the multimachine database from which the scaling equation given at the beginning of this paragraph was derived. Data from many machines (including the large ST, MAST), with different machine sizes, geometries, and fueling variations have already been included in the database and the scaling.

The threshold studies showed that there were other factors that affected the L–H transition power threshold on NSTX which have yet to be fully understood. These factors included wall conditioning, plasma impurity content, magnetic configuration, and fueling rate and location. For $I_p = 900$ kA, the NBI power required at threshold was reduced from 830 kW to 660 kW following 350 °C bake-out, boronization, and error field correction.

IV. FLUCTUATIONS BEFORE DURING AND AFTER THE L–H TRANSITION

Fluctuations were reduced in the edge plasma at the transition and during the H-mode, including the scrape off layer (SOL) and the steep density gradient regions. Fluctuation data for the SOL were provided by the gas puff imaging (GPI) diagnostic,[16] the reciprocating edge probe, and the broadband from 6 to 26 GHz (6–26 GHz) reflectometer.[17] Data for the steep density gradient region were provided by the edge scanning reflectometer. Figure 11 shows density fluctuation power spectra from the 6–26 GHz reflectometer for the L-mode and H-mode phases of a typical discharge. Comparison of the two spectra taken in the SOL, where $T_e < 20$ eV and $n_e < 3 \times 10^{12}/cm^3$, demonstrated that the turbulence was reduced in the SOL during the H mode. The H-mode spectrum was far below that for the L-mode for the full frequency range shown; 10 to 500 kHz. The greatest difference was in the 100 to 500 kHz range with a difference of greater than two orders of magnitude at 300 kHz. A strong coherent mode at a frequency slightly greater than 100 kHz was evident in the H-mode spectrum.

The fast edge scanning reflectometer[18] also showed fluctuations to be reduced after the L–H transition. Figure 12 shows the results for this diagnostic. Spectrograms of the density fluctuations are shown at three different density locations (cutoffs); $3.8 \times 10^{12}/cm^3 (f = 17.6 \text{ GHz})$, $9.9 \times 10^{12}/cm^3 (f = 28.2 \text{ GHz})$, and $3.1 \times 10^{13}/cm^3 (f = 50 \text{ GHz})$. At the transition, all three spectrograms showed an instantaneous reduction in the fluctuations for frequencies above approximately 50 kHz. All three spectrograms showed a temporary return of fluctuations due to an event (most likely an ELM) at ~ 0.334 s. At the steep density gradient position at $\sim 1 \times 10^{13}/cm^3$ the power spectrum for the H-mode phase (0.340–0.345 s) was an order of magnitude lower than the spectrum for the L-mode phase (0.325–0.330 s) through the full frequency range studied of 5 kHz to 1 MHz. This was found in the power spectra of the two cases but is not shown here. The H-mode spectrum showed an intermittent coherent mode at high frequency, 120 to 150 kHz, similar to the coherent mode centered at ~ 120 kHz in the spectrum for the 6–26 GHz reflectometer. Coherent modes have also been seen in high performance plasmas resulting from H-mode operation in some conventional aspect ratio tokamaks. These include the quiescent double barrier (QDB) mode[19] in DIII-D and the quasicoherent mode (QCM) observed in enhanced D_α (EDA) operation[20] in the C-Mod tokamak. The mode is likely not related to the edge harmonic oscillations (EHO) of the QDB mode since the frequency of the EHO is much lower (6–10 kHz). The frequency of the QCM is in the range 60–200 kHz and this is similar to the 100–150 kHz range for the NSTX coherent mode. The frequency of the NSTX mode is in the TAE gap and is most likely a TAE mode. On the other hand, a mode related to the QCM cannot be ruled out at this time.

The edge turbulence in the scrape off layer (SOL) during H-modes in NSTX was also measured using gas puff imaging (GPI),[16] in which the neutral line emission from a helium gas puff was imaged to determine the local space–time structure of the edge turbulence. In these experiments the gas injected was He and the HeI (587.6 nm) line was used for imaging. The temporal evolution of the 2D turbulence was measured within a 30 cm poloidal by 15 cm radial area centered 17° above the outer midline using a PSI-4 ultrahigh speed camera.[21] This was supplemented by time series data from discrete chord fiber optic arrays located within the image.

Normally, based on GPI data L-mode (and Ohmic) plasmas showed a complicated structure in the edge region, whereas H-mode plasmas usually have a less turbulent structure. Comparison of the poloidal k spectrum based on GPI measurements in NSTX of an L-mode (#108322) and quiescent H-mode discharge (#108316) is shown in Fig. 13. The shapes of the k spectra are similar but the fluctuation level in the H-mode is $\approx 3–4$ times lower in this case. These spectra were evaluated at the plasma edge ($r/a \approx 0.95–1.0$) where Te$\approx 10–15$ eV in both cases.

Just as in L-mode plasmas, H-modes in NSTX can have localized "blobs"[22] moving radially or poloidally within the edge region, similar to structures recently seen at Alcator C-Mod.[23] These blobs appeared as local maxima in the 2D
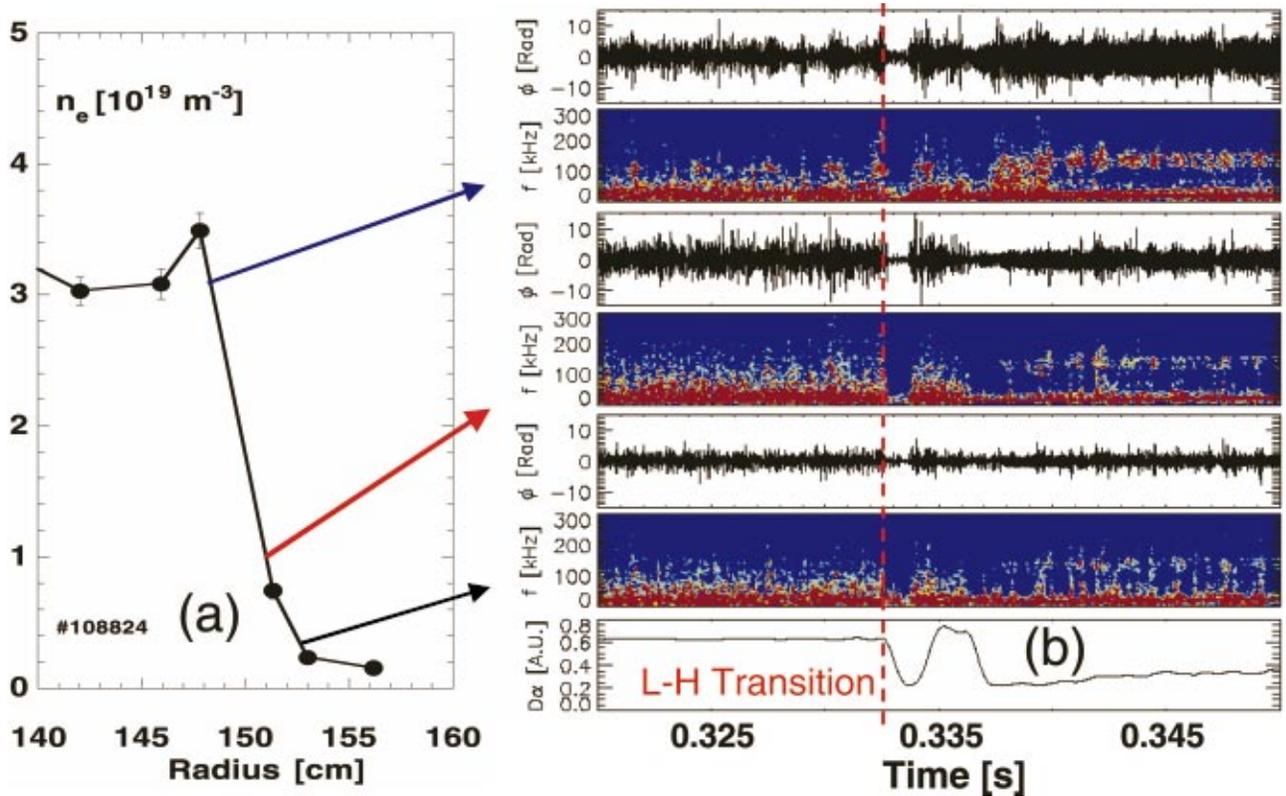
FIG. 12. (Color) Spectrograms from the fast scanning edge reflectometer for fluctuations before, during, and after the L–H transition. The fluctuations went away at the transition and except for a single ELM burst, remained suppressed, especially at the steep density gradient position in the plasma.

images and as large transient spikes in the discrete chord time series. It is interesting to note that these transient spikes were apparently not related to the ELMs that occurred during NSTX H-mode plasmas, since the spikes seen in the GPI chord signals could occur between ELMs (and seemed to be reduced during ELMs). Similar intermittent events caused significant local particle transport during the H-mode in DIII-D.[24]

V. ELM BEHAVIOR AND CHARACTERISTICS IN NSTX

ELMs are of interest to NSTX for several reasons. First, determining and quantifying their effects on the plasma itself

FIG. 13. Data from GPI diagnostic comparing poloidal k-spectra for an L-mode and a quiescent H-mode edge plasma. Shows fluctuation level in H-mode is 3 to 4 times lower than in L-mode in the SOL.

may help to gain an understanding of ELM physics. Second, ELM behavior must be controlled in order to employ them to modify plasma properties, e.g., restricting core impurity accumulation, and edge density control. Third, and associated most with fundamental physics of H-modes, were the ELM effects on the edge pedestal. Recent studies in tokamaks[25] showed that the edge pedestal (n,T,p) affects the core confinement in a dynamic fashion. Changes in edge pedestal height and width impacted core confinement essentially instantaneously. Therefore, the ELM studies in NSTX included preliminary determination of the parametric dependence of ELM perturbations such as $\Delta n_e/n_e$, $\Delta T_e/T_e$, $\Delta T_i/T_i$, $\Delta V_\phi/V_\phi$, and $\Delta W/W$ at each ELM. Machine parameters, I_p, B_t, n, T, and V_p affect the size and radial extent of ELM perturbations. As a component of the push to higher β operation, one strategy would be to tailor the ELM size and frequency to modulate the edge pressure without significant de-rating of the overall plasma performance. This could help to avoid exceeding stability limits that lead to large ELMs that dump large portions of plasma particles and energy and cause localized divertor plate heat loading (hot spots). So far, there appear to be few qualitative differences in ELM behavior between low aspect ratio STs and conventional aspect ratio tokamaks.

A variety of ELMs were observed on NSTX, and ELMs were obtained in both LSN and DN divertor configurations. DN divertor plasmas ELM easily while LSN divertor plasmas do not. Very often, the LSN H-modes were ELM free or have long period intermittent giant ELMs.
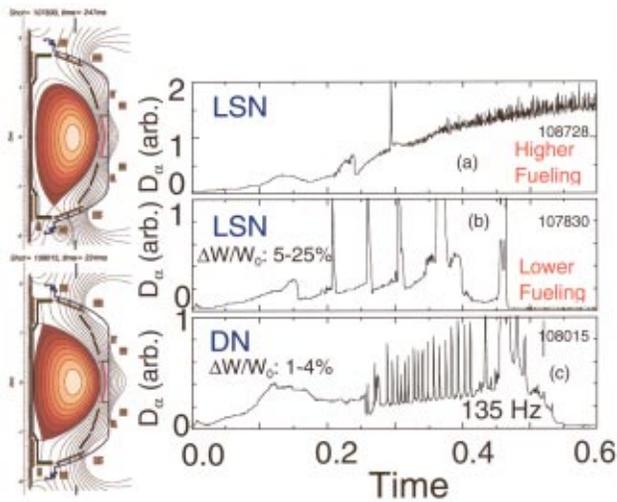
FIG. 14. Variety of ELM behavior with configuration and operating parameters (a) ELM-free in LSN divertor, (b) giant ELMs in LSN divertor, and (c) ELMs of modest amplitude and frequency in DN configuration.

On NSTX the ELM behavior depended on operating conditions and divertor configuration. Factors that influenced ELM behavior included, edge density and temperature, toroidal field, heating power magnitude and type, gas puff flow rate, and magnetic geometry. This is illustrated in Fig. 14, which shows the ELM behavior for three different discharges.

Figures 14(a) and 14(b) show two different types of ELM behavior in the LSN divertor configuration, and Fig. 14(c) is a DN divertor example. In Fig. 14(a) the D_α signal
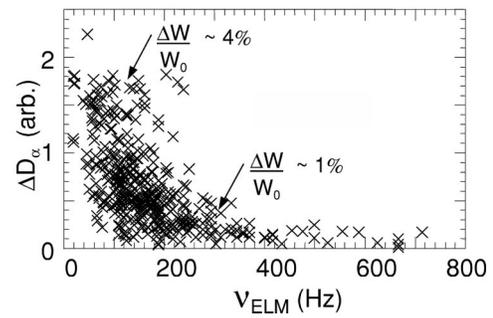
FIG. 15. Plot of ELM amplitude, ΔD_α versus ELM frequency ν_{ELM}.

shows the plasma was virtually ELM free. However, there were high frequency fluctuations that were superimposed on the D_α signal for the duration of the H-mode. We have not yet conclusively identified the fluctuations as high frequency ELMs or oscillations similar to those observed during high performance plasmas in conventional aspect ratio tokamaks.

Giant ELMs occurred in the second LSN case, which had, among other differences, a lower fueling rate. In the third case, for the DN divertor, the ELM frequency was high and the amplitude modest. A database of ELM parameters was assembled and in general it was found that ELM amplitude decreased with increasing frequency. This is evident in Fig. 15, which is a plot of the amplitude of the D_α burst, ΔD_α, during an ELM, versus frequency ν_{ELM}. Here, ν_{ELM} is $1/\Delta t$ ELM to ELM. As shown in Fig. 15, ΔD_α decreased strongly as ν_{ELM} increased. This frequency behavior is consistent with type I ELMs on conventional tokamaks. In
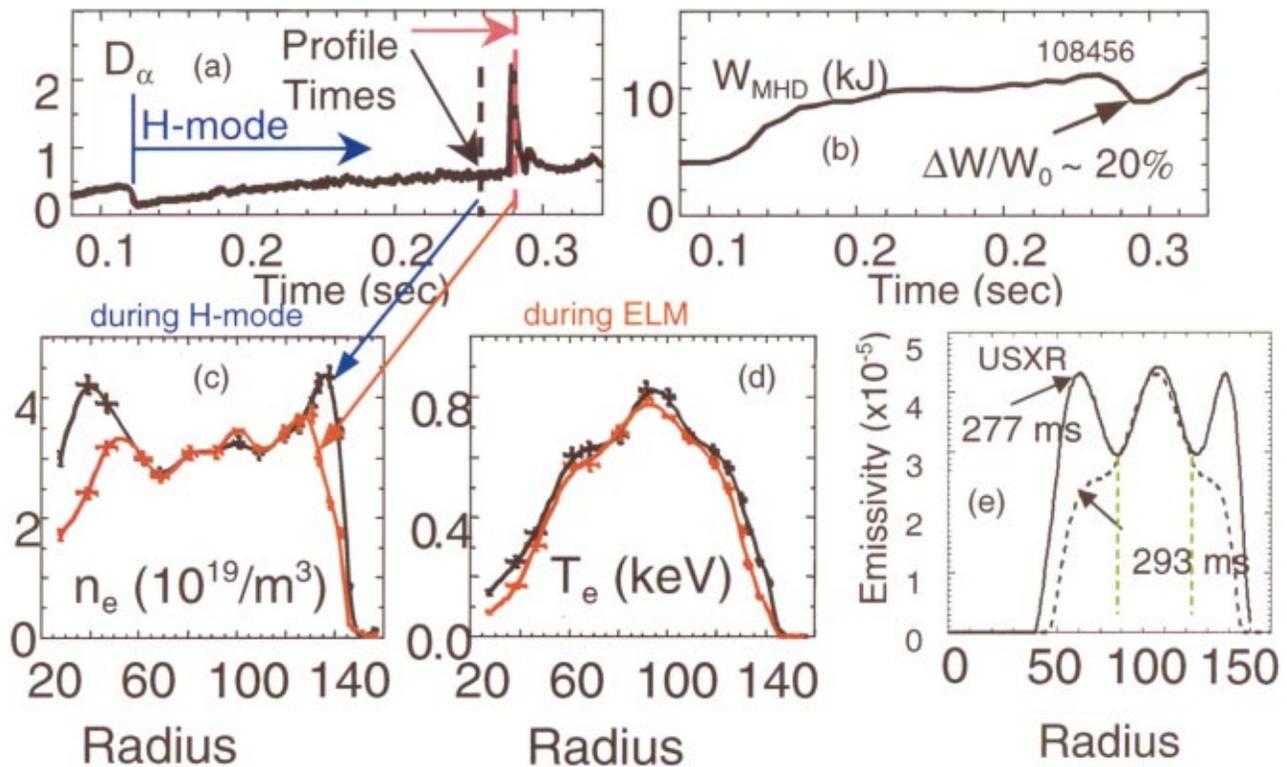
FIG. 16. (Color) Parameters and profiles for a giant ELM showing effect extends deep into the plasma core. (a) D_α signal, (b) W_{MHD} is stored energy, (c), (d), (e) include n_e, T_e, and USXR emissivity profiles before and during the ELM.
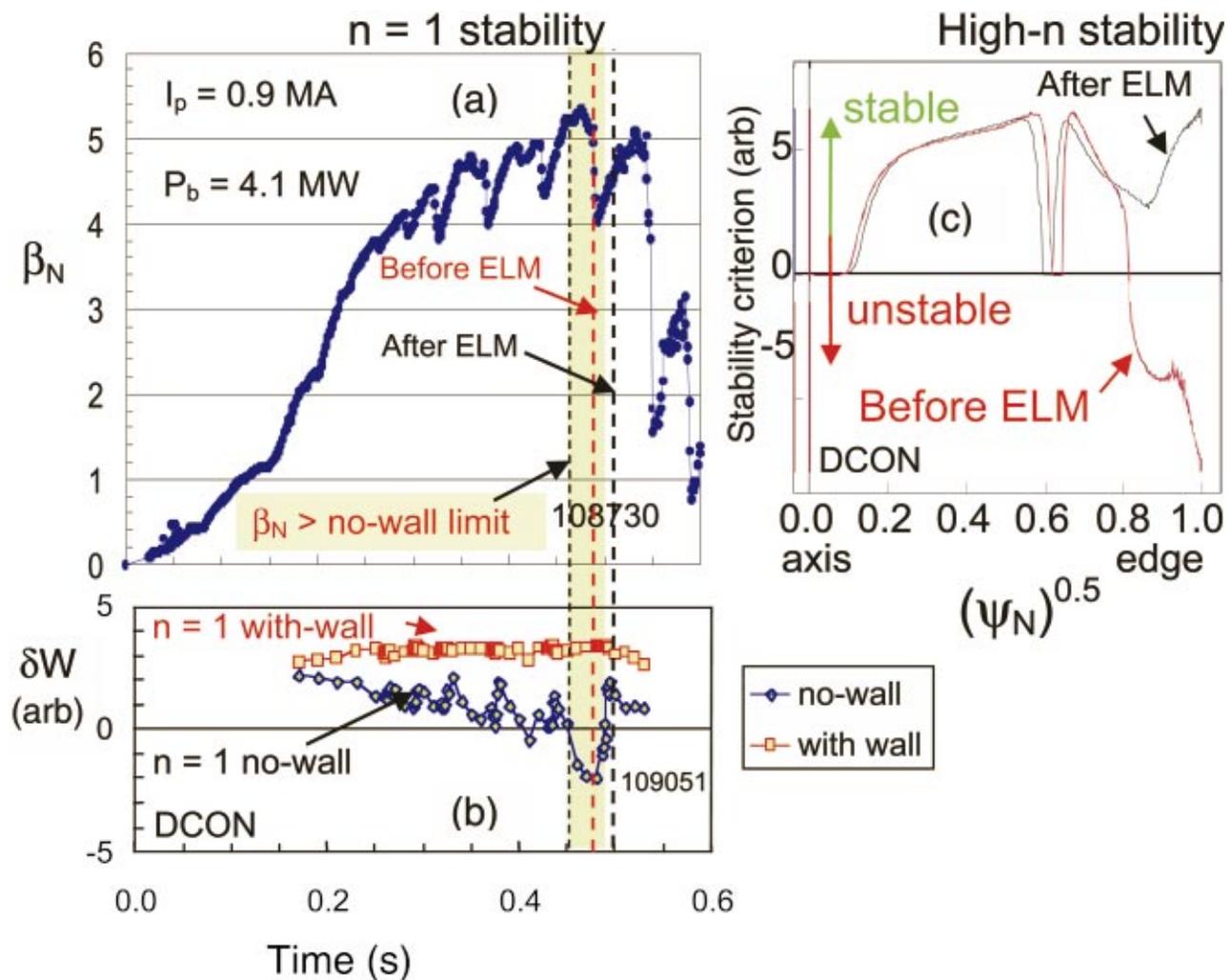
FIG. 17. (Color) Results of a stability analysis for a plasma with a train of four giant ELMs. Plasma was high-n ballooning unstable just before the fourth ELM but stable after the ELM. The $n=1$ kink mode was wall stabilized and not responsible for the ELM.

NSTX the giant ELMs were observed in LSN H-modes with medium β, medium triangularity, and low fueling. This is different from conventional aspect ratio tokamaks where the largest ELMs occur in H-mode plasmas, which are the most strongly shaped, have the highest β's, and performances. Additional work must be done to explain the NSTX giant ELM result.

The ELM size and frequency also affected the extent to which the H-mode character was temporarily lost afterwards. Large ELMs as in Fig. 14(b) very often appeared to return confinement to L-mode. In fact, the L-mode edge immediately following the ELM seemed to cause an instant transition back to the H mode, with the D_α signal falling below its original level just before the ELM (H-mode phase) as seen just after the three large ELMs of Fig. 14(b). The fourth burst on the D_α trace was the result of an internal mode that destroyed confinement and terminated the H mode. For more modest ELMs, as in Fig. 14(c), the effect was restricted to a thin shell of plasma and performance was only slightly reduced relative to ELM-free operation. It is important to note that a much wider variety of ELM behavior was observed on NSTX than illustrated in Fig. 14.

For a plasma in which a single giant ELM occurred (shown in Fig. 16) the "ears" on the n_e profile [Fig. 16(c)] were completely lost, reducing n_e at the edge (e.g., $R \sim 1.40$ m) to $\sim 50\%$ of its prior H-mode value. The D_α signal of Fig. 16(a) shows the L–H transition at $t=0.12$ s and giant ELM at $t=0.28$ s. The magnitude and radial extent of the ELM perturbation were also reflected in USXR array emissivity [Fig. 16(d)]. The emissivity in a broad shell fell to essentially zero; only a 15 cm radius region of the core was unaffected as seen in Fig. 16(e). The USXR emission in Fig. 16(e) varies as $f(T_e) \cdot n_e^2 \cdot Z_{eff}$ in the ordering $f(T_e) > n_e > Z_{eff}$. Thus the x-ray emissivity profile shape is dominated by the density and temperature profile shapes, and changes from the emissivity profile before the ELM to the profile after the ELM are due predominantly to changes in these parameters and not to large changes in Z_{eff}. Just before the transition the bulk of the emission is from photons in the range 1.8 to 2 keV. Large radial extent and stored energy loss during large ELMs have also been observed on conventional aspect ratio tokamaks.[26] The implications for the next step ST then would be the same as for conventional aspect ratio

tokamaks, in that large concentrated wall heat loading would result from large ELM activity. Also, the loss of energy would lead to loss of reactivity.

A stability analysis[27,28] (Fig. 17) of a similar discharge showed the plasma to be high-*n* ballooning unstable and low-*n* stable before some giant ELMs. A large fraction of the plasma was high-*n* ballooning unstable just before the final ELM [Fig. 17(c)]. In addition, the plasma was low-*n* kink unstable without a wall, but stable in the presence of the NSTX conducting wall. It is likely therefore that high-n ballooning was responsible for the instability.

VI. SUMMARY AND CONCLUSION

The NSTX H modes enabled access to reproducible high performance plasmas with separately achieved H-phase durations >500 ms and β_T up to 35%. Both L-mode and H-mode confinement were enhanced relative to the τ_E^{97L} scaling, having a nominal enhancement factor of $H_{97L} \sim 1.5$, ranging from 0.75 to 2.5 times the 97L scaling.

The NSTX H modes were found to have similarities to those of conventional aspect ratio tokamaks, with some notable exceptions. The H-mode power threshold in NSTX was found to be about 2.5 to 6 times higher than a recent international scaling.[15] There was a clear I_p dependence of the power threshold for the L–H transition, and this is different from conventional aspect ratio tokamaks. ELM behavior was dependent on configuration and fueling and a wide variation in ELM characteristics was observed. Fluctuation levels were reduced in the SOL and at the steep gradient region of the n_e profile at the transition. This is consistent with an edge transport barrier. Thus, routine access to H-modes is facilitating studies of high β and long pulse in NSTX.

ACKNOWLEDGMENTS

[1] C. Neumeyer, P. Heitzenroeder, J. Spitzer *et al.*, Fusion Eng. Des. **54**, 275 (2001).
[2] C. E. Bush *et al.*, Proceedings of 29th European Conference on Plasma Physics and Controlled Fusion, Montreaux, SZ, 17–22 June 2002.
[3] R. Maingi, M. G. Bell, R. E. Bell *et al.*, Plasma Phys. Controlled Fusion **45**, 657 (2003).
[4] D. Mueller, M. Ono, M. G. Bell *et al.*, "Results of NSTX Heating Experiments," Proceedings of the 29th International Conference on Plasma Science, Alberta, CA, June 17–22, 2002, Trans. Plasma Sci. (accepted).
[5] D. A. Gates, Bull. Am. Phys. Soc. **47**, 18 (2002).
[6] B. P. LeBlanc, M. G. Bell, R. E. Bell *et al.*, "Confinement studies of auxiliary heated NSTX plasmas," 19th IAEA Fusion Energy Conference, Oct. 14–19, 2002, Lyon, France, paper IAEA-CN-94/EX/C5-2.
[7] H. W. Kugel, V. Soukhanovskii, M. Bell *et al.*, "Impact of the wall conditioning program on plasma performance in NSTX," PPPL Report No. PPPL-3725, July 2002, Proceedings of the 15th International Conference on Plasma Surface Interactions in Controlled Fusion Devices, 27–31 May 2002, Gifu, Japan.
[8] A. R. Field, P. G. Carolan, R. J. Akers *et al.*, Plasma Phys. Controlled Fusion **44**, A113 (2002).
[9] R. Maingi, M. G. Bell, R. E. Bell *et al.*, "H-mode Research in NSTX," Nucl. Fusion (submitted).
[10] ITER Physics Basis Editors, Nucl. Fusion **39**, 2175 (1999).
[11] R. Maingi, M. G. Bell, R. E. Bell *et al.*, Phys. Rev. Lett. **88**, 035003 (2002).
[12] C. E. Bush, R. Maingi, M. G. Bell *et al.*, Plasma Phys. Controlled Fusion **44**, A323 (2002).
[13] A. Sykes, J.-W. Ahn, R. Akers *et al.*, Phys. Plasmas **8**, 2101 (2001).
[14] J. A. Snipes *et al.*, Proceedings of the 24th European Physical Society Conference on Controlled Fusion and Plasma Physics, Berchtesgaden, Germany, 1997, Geneva, Part III, p. 961.
[15] J. A. Snipes *et al.*, "Multi-machine global confinement and H-mode threshold analysis," IAEA 2002 paper CT/P-04 to be published on CD-ROM and the World Wide Web.
[16] R. Maqueda, G. A. Wurden, D. P. Stotler *et al.*, "Gas puff imaging of edge turbulence" Rev. Sci. Instrum. (accepted).
[17] J. B. Wilgen, G. R. Hansen, T. S. Bigelow, D. W. Swain, P. M. Ryan, M. D. Carter, J. R. Wilson, and the NSTX Team, Bull. Am. Phys. Soc. **46**, 259 (2001).
[18] S. Kubota, X. V. Nguyen, W. A. Peebles, L. Zeng, and E. J. Doyle, Rev. Sci. Instrum. **72**, 348 (2001).
[19] K. H. Burrell, M. E. Austin, D. P. Brennan *et al.*, Phys. Plasmas **8**, 2153 (2001).
[20] M. Greenwald, R. Boivin, P. Bonoli *et al.*, Phys. Plasmas **6**, 1943 (1999).
[21] Princeton Scientific Instruments, 7 Deer Park Drive, Monmouth Junction, NJ.
[22] S. J. Zweben, R. Maqueda, D. Stotler *et al.*, "High speed imaging of edge turbulence in NSTX," Nucl. Fusion (submitted).
[23] J. L. Terry, Bull. Am. Phys. Soc. **47**, 183 (2002).
[24] J. A. Boedo, Bull. Am. Phys. Soc. **47**, 183 (2002).
[25] R. J. Groebner, D. R. Baker, K. H. Burrell *et al.*, Nucl. Fusion **41**, 1789 (2001).
[26] S. M. Kaye, J. L. Dunlap, H. Kugel, B. LeBlanc, L. Schmitz, S. Sesnic, and G. Tynan, Plasma Phys. Controlled Fusion **36**, A51 (1994).
[27] S. A. Sabbagh, R. E. Bell, M. G. Bell *et al.*, Phys. Plasmas **9**, 2085 (2002).
[28] A. H. Glasser and M. S. Chance, Bull. Am. Phys. Soc. **42**, 1848 (1997).